Optics & Laser Technology 167 (2023) 109713

Contents lists available at ScienceDirect

Optics and Laser Technology

journal homepage: www.elsevier.com/locate/optlastec

Full length article

Spectroscopic and lasing characteristics of Yb:YGG at cryogenic temperatures

Sami Slimi [a], Venkatesan Jambunathan [b], Ghassen Zin Elabedine [a], Haohai Yu [c], Huaijin Zhang [c], Weidong Chen [d], Rosa Maria Solé [a], Magdalena Aguiló [a], Francesc Díaz [a], Martin Smrz [b], Tomas Mocek [b], Xavier Mateos [a,e,*]

[a] Universitat Rovira i Virgili (URV), Física i Cristal·lografia de Materials (FiCMA), Marcel·lí Domingo 1, 43007 Tarragona, Spain
[b] HiLASE Centre, Institute of Physics of the Czech Academy of Sciences, Za Radnicí 828, 252 41 Dolní Břežany, Czech Republic
[c] State Key Laboratory of Crystal Materials, Shandong University, Jinan 250100, China
[d] Fujian Institute of Research on the Structure of Matter, Chinese Academy of Sciences, Fuzhou 350002, Fujian, China
[e] Serra Húnter Fellow

ARTICLE INFO

Keywords:
Gallium garnet crystals
Yb^{3+} ions
Spectroscopy
Cryogenic lasers

ABSTRACT

We report on the optical spectroscopy and continuous-wave (CW) laser operation of ytterbium-doped yttrium gallium garnet (Yb:YGG) crystal at cryogenic temperatures. A maximum absorption cross-section of 1.7×10^{-20} cm^2 with spectral bandwidth of 2.4 nm centered at 970.5 nm and a maximum emission cross-section of 6.5×10^{-20} cm^2 with spectral bandwidth of 4.6 nm centered at 1024 nm were determined at 120 K. Cryogenic continuous-wave laser operation was achieved using a VBG stabilized laser diode emitting around 969 nm as pump source. At 120 K, a maximum output power of 17.50 W was achieved around 1024 nm corresponding to a slope efficiency of 87% with respect to the absorbed power.

1. Introduction

Ytterbium-doped gain medium is an admittedly efficient solid-state laser material, which has precious applications in many fields [1,2]. In comparison to conventional Nd^{3+} ion lasers, Yb^{3+} ion lasers emitting at ~ 1 μm offer certain advantages, such as a simple energy level scheme which eliminates undesirable upconversion and excited-state absorption processes, low heat transfer to the host and high efficiency due to the small quantum defect, which leads to a reduction in thermal load and offers attractive power-scaling capabilities; lack of excited-state absorption and concentration quenching [3]; and wide absorption and emission bands that not only support flexible diode pumping requirements but also enable generation of ultrashort laser pulses via the mode-locking technique [4–6].

During the past two decades, great attention has been paid to the exploration and development of Yb^{3+} laser hosts. A variety of hosts have been studied, and crystals belonging to the family of garnets, with general chemical formula $\{A\}_3[B]_2(C)_3O_{12}$ (where A = Ca, La, Y, Gd or Lu, B = Al, Ga, Fe, Sc and C = Al, Fe, Ge, or Ga), proved to be promising for high power laser applications, mainly because of their good thermo optic and thermo mechanical properties [7–9]. Garnet crystals, like the well-known Yb:YAG laser, are suffering from low transition cross-sections, one example is the required multipass pumping in Yb -based thin-disk lasers to have enough absorption. The approach of cooling the active medium to cryogenic temperatures partially overcomes the aforementioned issues with reabsorption and low transition cross-sections. The transition cross-sections increase at low temperatures. In addition, at cryogenic temperatures, the thermo-optical properties are enhanced. Thermal conductivity rises while thermal expansion and thermal dependency of the refractive index (dn/dt) decrease considerably. All of these factors have positive impact on minimizing the thermal lensing effect that occurs in the active medium when subjected to laser pumping. The improvement in thermo-optical properties results in higher laser efficiencies, especially the optical–optical efficiency in relation to the lower laser threshold, and also facilitates the scalability of the average output power [3,10,11].

Gallium garnets with general chemical formula $RE_3Ga_5O_{12}$ (REGG) where RE = Gd, Y, or Lu, possess ordered structure where Yb ions replace RE ions in a single crystallographic site with low symmetry. These crystals are usually grown by the optical floating zone method

* Corresponding author at: Universitat Rovira i Virgili (URV), Física i Cristal·lografia de Materials (FiCMA), Marcel·lí Domingo 1, 43007 Tarragona, Spain.
E-mail address: xavier.mateos@urv.cat (X. Mateos).

https://doi.org/10.1016/j.optlastec.2023.109713
Received 3 April 2023; Received in revised form 17 May 2023; Accepted 5 June 2023
Available online 22 June 2023

[12] and Czochralski technique [8]. Large volume and highly doped crystals (10 at.% Yb) with good optical uniformity can be attained. The thermal conductivity of ~ 7 at.% doped Yb:REGG is ~ 5 W/mK and their physical properties are usually similar to those of YAG [13]. The spectroscopic properties of Yb^{3+} ions in REGG have been previously studied [12,13] at room temperature (RT). Also, at RT, continuous wave (CW), Q-switched, and mode-locked operation with Yb:REGG crystals has also been documented [14–17]. Passively Q-switched laser action of such Yb -doped gallium garnets was also demonstrated by utilizing single layer graphene saturable absorber, with pulse energy limited to about 2 μJ and with pulse durations being as long as several hundreds of nanoseconds [18]. Ytterbium-doped the cubic yttrium gallium garnet crystal (shortly abbreviated YGG) is known for decades but poorly investigated as compared with other garnets crystals such as Yb:(Y, Lu)AG crystals. The early studies of that crystal focused on the crystal growth and the RT spectroscopy [12,19]. Later on, laser actions and were reported [16–18]. To date, many Yb-doped garnet laser hosts have been investigated at cryogenic temperatures [20–23], while little consideration has been placed on Yb-doped gallium garnets. In this paper, we present a detailed study on the spectroscopic characteristics of this crystal in regard to absorption and emission cross-sections have been explored at different cryogenic temperatures. In addition, the continuous-wave laser operation at several cryogenic temperatures has also been demonstrated.

2. Experimental

The absorption spectra were measured using a Varian CARY 5000 spectrophotometer with variable slit widths (down to 0.01 nm) for optimal control of data resolution. We used a 400 μm thick sample. The low temperature measurements were carried out using a cryostat (Oxford Instruments, model SU 12) with helium-gas close-cycle flow. The luminescence spectra were measured using an optical spectrum analyzer (OSA, Hamamatsu, AQ6373) characterized by a spectral resolution that can vary from 0.02 to 10 nm, the pump source was a fiber coupled laser diode (BWT Beijing LTD) emitting unpolarized radiation at 968.87 nm. The luminescence lifetime was measured at different temperatures using a mechanically modulated InGaAs diode pump source emitting around 968 nm. An Optical Spectrum Analyser, OSA and a 2 GHz Tektronix DPO5204B digital oscilloscope were used to collect the emission from the crystal.

Laser experiments were carried out on an uncoated 7.35 at % Yb: YGG garnet single crystal having a thickness of 6 mm and an aperture of 3 × 3 mm^2. We employed a ~75 mm long L-shaped cavity consisting of several optical elements: a dichroic mirror (DM), a plano-concave mirror (ROC = 300 mm) HR coated for laser wavelength (1020–1070 nm), a plano-convex lens (f = 150 mm) AR coated for laser wavelength and a flat output coupler mirror (HR coated @1030 nm) with partial transmission. The front face of the DM was HR coated for laser wavelength whereas its rear face was AR coated to completely allow the pump beam. The schematic diagram of the experimental setup is shown in Fig. 1. As a pump source, we used a 60 W laser diode (BWT Beijing LTD) whose wavelength was locked at 968.8 nm with a narrow spectral bandwidth of 0.40 nm by an integrated volume Bragg grating (VBG) element. The pump laser light was coupled with the fiber having a core diameter of 105 μm and an NA of 0.22. Pump radiation was imaged on the crystal sample in 1:2.5 ratio using achromatic lenses with antireflection coating for pump wavelength, the size of the produced pump spot of ~ 262 μm.

The uncoated laser element was pumped in a single-pass configuration. It was wrapped in an indium foil and was mounted in a copper holder at normal incidence and fixed to the cold finger of the optical cryostat providing a heat load of 13 W at 100 K. To achieve and regulate cryogenic temperatures of the sample between 80 and 200 K, a helium cooled closed cycle cryostat (Cryogenics of America: Model No.CH-204SFF) and a 50 Ω resistor heater along with a temperature controller (LakeShore - Model No. 335) were used. The temperatures were measured on the cold finger using a Si diode sensor (DT-670, LakeShore).

Output couplers with different transmissions (TOC = 10, 20, 30, 40 and 50%) were employed for this study and at different sample temperatures from 80 to 200 K with an interval of 20 K. The distances of the cavity optics were tuned to achieve maximum output power with good beam quality having a Gaussian distribution intensity profile. Based on the optimized cavity distances and the ABCD formalism, the laser mode size was calculated to be ~222 μm in the crystal. The laser output was filtered from the residual pump using a long-pass filter (FEL1000, Thorlabs) and the laser emission spectra were then measured using an Ocean Optics compact spectrometer (model USB 2000 +).

3. Results and discussion

3.1. Cryogenic spectroscopy

The absorption spectra were measured at different temperatures in the range 850–1050 nm. For the sake of brevity, only few temperatures are reported (300 K, 200 K and 100 K). The absorption cross-sections σ_{abs} were obtained using Lambert–Beer's law which relates the spectral intensity of the white light source I(λ), transmitted through the sample, to the spectral intensity $I_0(\lambda)$ measured without the sample inserted into the beam path, for each wavelength λ:

$$\sigma_{abs} = \ln\left(\frac{I_0(\lambda)}{I(\lambda)}\right) \Big/ N_{Yb} l \quad (2)$$

Here, N_{Yb} is the dopant ion density, which was determined to be 9.7 × 10^{20} atoms/cm^3, l the thickness of the sample. In general, the absorption cross-sections increase with decreasing in temperature. From Fig. 2(a) one can see that the absorption cross-section of the ZPL at 970.5 nm is 1.32 10^{-20} cm^2 at 300 K and it increased to 1.71 10^{-20} cm^2 when the temperature went down to 120 K. The absorption bandwidth near the ZPL is reduced from 3.1 nm at 300 K to 2.4 nm at 120 K. The absorption spectra between 918 and 945 nm are characterized by a wide

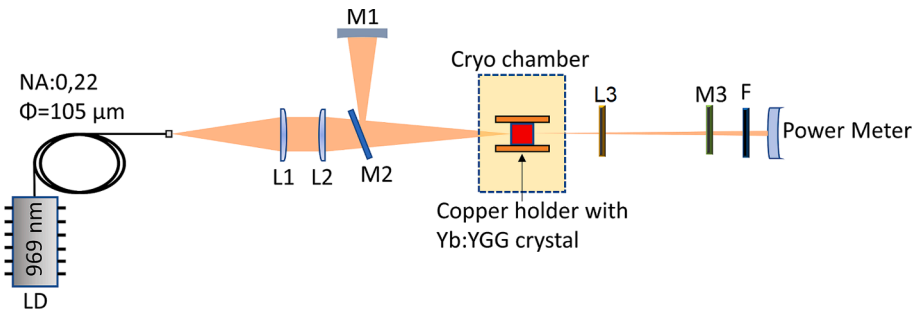

Fig. 1. Experimental laser setup. LD - laser diode emitting ~ 969 nm, core diameter 105 μm, N.A. = 0.22. L1&L2: Achromatic lenses with a ratio of L1:L2 = 1:2.5, M1: End Mirror HR 1030 nm, M2: Dichroic Mirror AR 900–980 nm HR & HR 1020–1200 nm, L3: Lens f = 150 nm AR 1030 nm, M3: Output coupler, F: Long-pass filter.

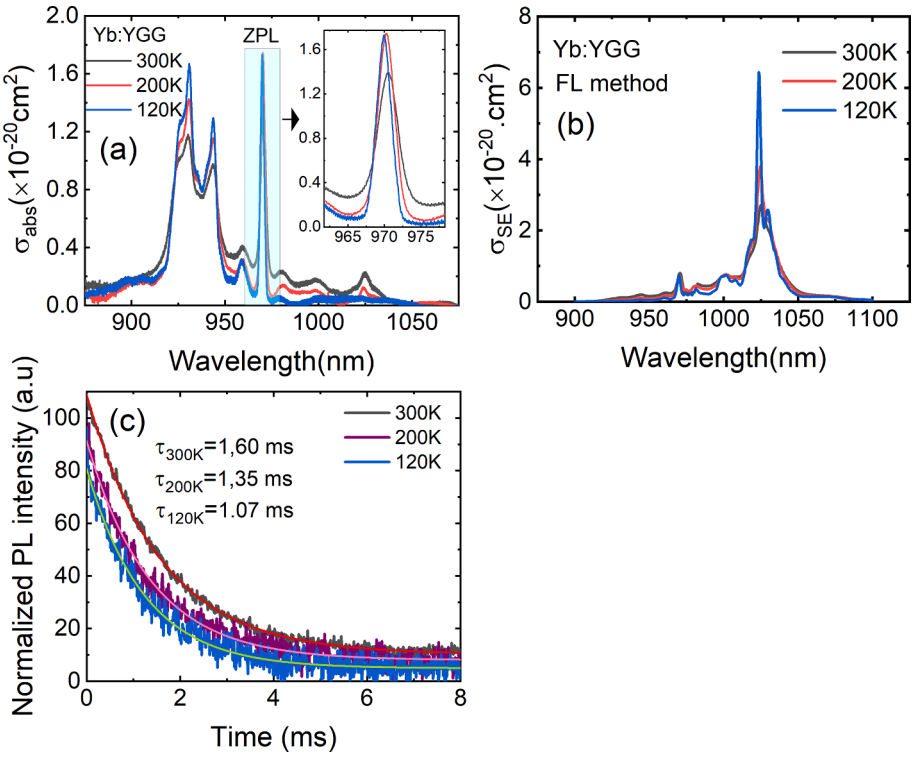

Fig. 2. Optical spectroscopy of 7.35 at % Yb:YGG garnet: Absorption with magnification of the Zero-phonon line (inset) (a) and emission (b) cross-sections at different temperatures; (c) luminescence lifetime at different temperatures, λ_{exc} = 969 nm and λ_{lum} = 1024 nm.

plateau, At RT, the value of absorption cross-section at 931 nm was 1.17 10^{-20} cm^2, which is very close to the one previously reported for 9.8 at.% Yb:YGG (1.25 10^{-20} cm^2, [12]). However, from the literature, the bandwidth of Yb:YAG near ZPL for temperatures ≤ 100 K was reported to be less than 0.2 nm [24]. Therefore, we expect that by using a pump source at ~ 969 nm at a temperature approaching 120 K, the pumping efficiency for Yb:YGG will be greater than that for Yb:YAG.

The luminescence spectra were collected at different temperature. The stimulated-emission (SE) cross-sections, σ_{SE}, at different temperatures, were calculated from the measured luminescence intensity calibrated for the spectral response of the set-up I(λ) using the Füchtbauer–Ladenburg (FL) formula [25]:

$$\sigma_{SE}(\lambda) = \frac{\lambda^5}{8\pi n^2 \tau_{rad} c} \frac{I(\lambda)}{\int \lambda I(\lambda) d\lambda} \quad (3)$$

where λ is the light wavelength, n is the refractive index (at 1030 nm, n is ~ 1.91), c is the speed of light, τ_{rad} = 0.92 ms is the radiative lifetime of the emitting level ($^2F_{5/2}$) in YGG crystal measured at 80 K. At this temperature, the luminescence of Yb^{3+} ions is free from reabsorption losses and the luminescence lifetime (τ_{lum}) becomes very close to τ_{rad} due to the fact that the luminescence quantum yield in this case is close to unity [26]. The results are shown in Fig. 2(b). At room temperature, a broader emission band in the range 1011 to 1050 nm and an emission peak centered around 1024 nm can be deduced. Furthermore, for a temperature of 120 K, the broad peak at 1028 nm splits into two narrow peaks at 1023.7 nm and 1029.6 nm. At this temperature, the maximum σ_{SE} is 2.5 times higher than that measured at RT, 2.6 10^{-20} cm^2 which is equal to the previously reported value [12]. Moreover, it can be observed that the absorption bandwidth and emission bandwidth (a crucial parameter for short pulse generation) decrease with decreasing temperature.

The luminescence decay was studied at different temperatures at a wavelength of ~ 1024 nm. The decay curve from the $^2F_{5/2}$ state is well fitted using a single-exponential law, $I_{lum}(t) = I_0 \exp(-t/\tau_{lum})$. The results are presented in Fig. 2(c). The measured luminescence lifetime decreases slowly and steadily with decreasing temperature and has a measured value of around 1.07 ms at 120 K. At RT, the luminescence lifetime for 7.35 at.% Yb:YGG was 1.60 ms which is quite long due to the presence of strong reabsorption. It is a bit shoter than the one measured for the 9.8 at.% doped sample, 1.78 ms [12].

For Yb^{3+} ions at RT representing a quasi-three-level laser scheme with reabsorption, gain cross-sections, $\sigma_{gain} = \beta\sigma_{SE}-(1-\beta)\sigma_{abs}$, are usually calculated to know the expected laser wavelength and the gain bandwidth. Here, $\beta = N_2(^2F_{5/2})/N_{Yb}$ is the inversion ratio and N_2 is the population of the upper laser level. The gain profiles for the Yb:YGG crystal for various temperatures with varied inversion ratio β are shown in Fig. 3(a), (b) and (c). At RT, the gain curves are smooth and broad, due to the strong electron–phonon interaction in the host. The gain bandwidth is as broad as 20 nm. It can be seen that the value of σ_{gain} increases with the population inversion ratio β, and when β = 0.15, the positive gain cross-section is achieved at ~ 1025.7 nm. At 50% population inversion, namely, β = 0.5, the maximum grain cross-section is about 0.66 × 10^{-20} cm^2. As the temperature goes lower, we can see that the gain curve becomes narrower and its cross-section increases. From Fig. 3(d), one can infer that the gain cross-section increases with a decrease in temperature for a given β = 0.3 for instance. The highest gain peak is centered at ~ 1023.7 nm for a sample temperature of 120 K. For higher temperatures, the gain shifts to longer wavelengths around ~ 1025 nm. According to these estimations, one can expect laser oscillation around ~ 1023 nm at 100 K irrespective of the losses in the cavity.

3.2. Cryogenic continuous-wave laser operation

Cryogenic CW laser experiments using the uncoated sample were carried out by pumping at ~ 969 nm as mentioned in the experimental section. Fig. 4(a) shows the output power versus incident pump power achieved using several output couplers with various transmissions (from TOC = 10% to TOC = 50%). The output power rises linearly without any sign of saturation or thermal rool over for all output couplers. A maximum output power of 17.50 W corresponding to a slope efficiency

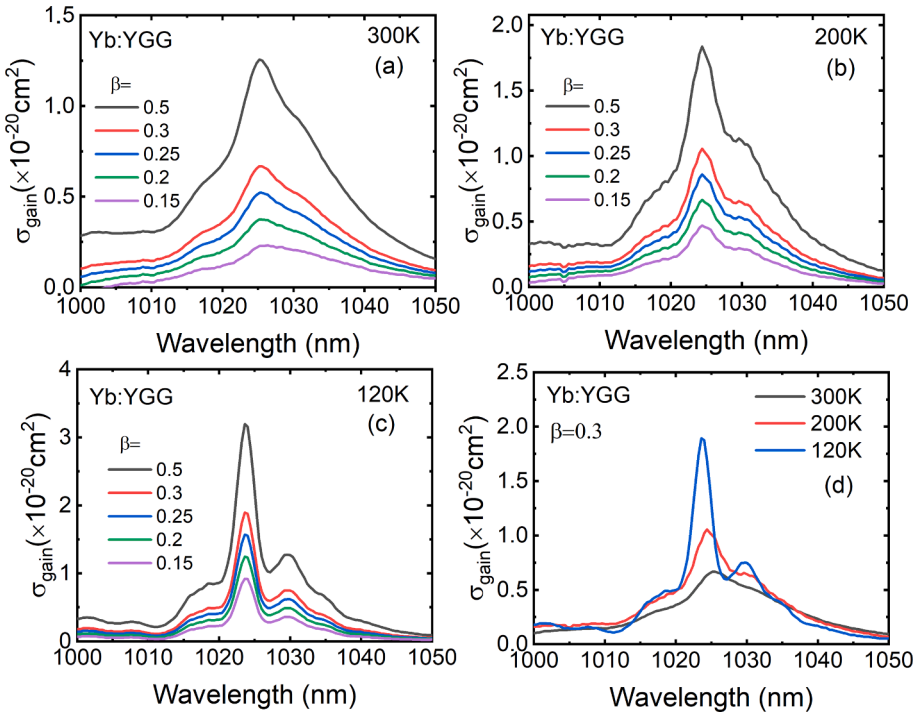

Fig. 3. Gain cross-sections of 7.35 at % Yb:YGG crystal in the 1000–1050 nm range for various temperatures and with several values of the inversion ratio β.

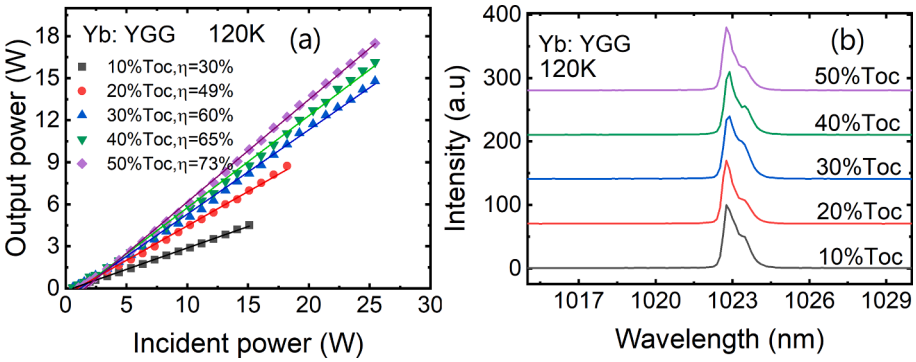

Fig. 4. Output power vs. incident power characteristics of the cryogenic Yb:YGG laser for different transmission of output coupling; (b) Laser emission wavelength at various TOC. The crystal temperature is fixed at 120 K and diode chiller temperature is maintained at 25 °C.

of 73% was achieved for a 50% transmission output coupling. The lasing threshold slightly increased as the output coupler transmission varies from 10 to 50% to be 0,596 to 1,053 W, respectively. The better efficiency and performance at higher output coupling can be ascribed to the high gain required at cryogenic temperatures. Out of the five different output couplers employed, the one with 10% transmission shows the lowest slope efficiency of 30% with a maximum output power of only 3.9 W. The beam profile was adversely affected for a TOC = 10% when it operated at the highest pump power. This is due to higher intra-cavity power under low coupling conditions. The laser wavelength was centered at 1022.7 nm in all cases, Fig. 4(b).

In the second part of our experiment, we characterized the laser performance at different cryogenic temperatures by fixing the output coupling to 50% and the heat-sink temperature of the diode to 25 °C. For the laser characterization, the sample temperature were varied from 80 K to 200 K in 20 K increments. Laser operation with crystal temperature above 200 K was not considered to avoid causing damage to the sample. Fig. 5.(a) shows the input–output characteristics of the cryogenic Yb: YGG laser by varying the sample temperature. A maximum slope efficiency of 73% was obtained at 120 K while an efficiency of only 33% was achieved at 200 K with an output power of 3.05 W. Fig. 5.(b) shows the trend of slope efficiency and laser threshold as a function of incident power at different temperatures. It is inferred that the slope efficiency is increasing, and the laser threshold is decreasing with the decrease in temperature. In comparison to 200 K, the efficiency is more than twice as high, and the output power is 5 times greater for the laser operating at 120 K. It was noted that by further reducing the temperature to 80 K, there was a small drop in efficiency (69%). A small change in absorption with respect to the shift and narrowing of the absorption band at much lower temperatures (less than100 K) may be accountable for a slightly lower efficiency at 80 K. This is a clear proof of a reduction in reabsorption losses. Therefore, it can be concluded that the significant improvement on the laser performance is due to both, the reduction of reabsorption due to four-level system and an enhancement material properties at cryogenic temperatures.

As a comparison of the obtained cryogenic laser performance for Yb: YGG crystal with other studied garnet materials, a similar cryogenic laser operations using the same design with L-shaped cavity were reported using Yb:GdYAG ceramic and Yb:LuAG garnet crystals [20,22], a maximum output power near 10 W was achieved for Yb:LuAG crystal

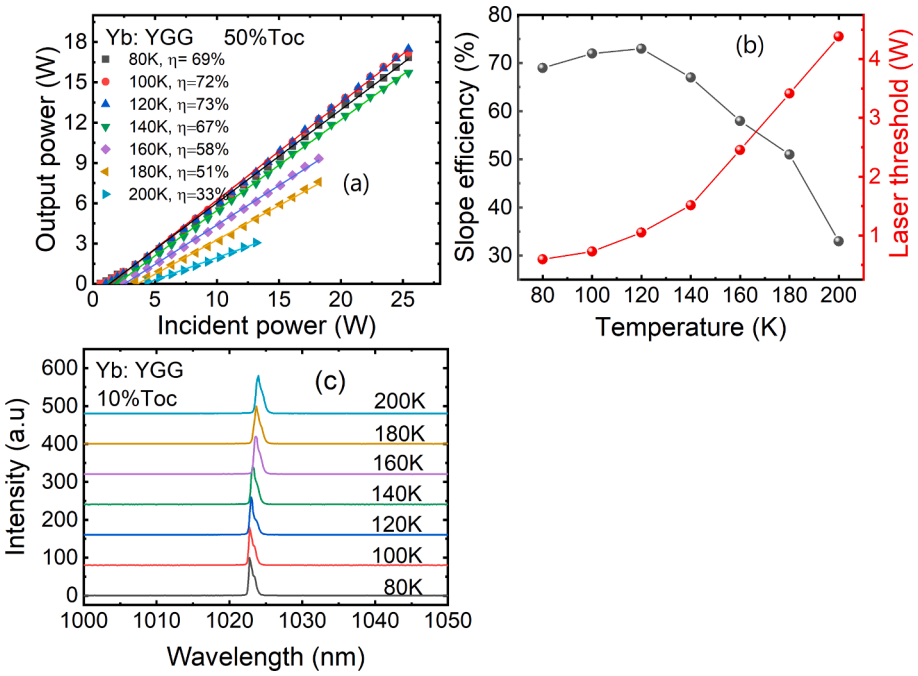

Fig. 5. (a) Output power vs. incident power characteristics of the cryogenic Yb:YGG laser for various crystal temperatures. The output coupler transmission is fixed to TOC = 50% and the diode heat-sink temperature fixed at 25 °C; (b) Output laser wavelength of cryogenic Yb:YGG laser for various sample temperatures.

with an optical-to-optical slope efficiency of 62%. While for Yb:GdYAG ceramic material, the efficiency was quite low with a maximum power equal to 2.92 W with efficiency of 20.3%.

We did not observe any saturation of the output power for all measurements performed at different temperatures. Under the given experimental conditions, 120 K was proven to be an optimum cooling temperature. The laser wavelength varied from 1023.9 to 1022.7 nm when the Yb:YGG crystal was cooled from 200 K to 80 K, Fig. 5.(c).

To judge the effect of pump absorption in the crystal, it was then measured under non-laser conditions as a function of the incident pump power for different crystal temperatures, as illustrated in Fig. 6(a). The absorption at 120 K was 84 %. It can be seen that the pump absorption in the crystal is lower at low incident pump power for temperatures below 120 K. This could be due to the shift in the pump wavelength as the laser diode current level increases, leading to a mismatch between the pump emission from the laser diode and the absorption band of Yb:YGG. A meaningful reduction in the absorption power is observed at a temperature below 120 K due to the narrowing of the absorption band, as shown in Fig. 6(b).

With the measured absorption of 84% at 120 K, we plotted the absorbed/output power characteristic in comparison with the incident/output power characteristic, as illustrated in Fig. 7.(a). The maximum output power of 17.5 W was achieved at an absorbed pump power of 18.5 W, which gives an optical-to-optical efficiency of 73%. The slope efficiency with respect to the absorbed power amounts to 87%. The laser beam is shown in Fig. 7.(b), which is shows an excellent far field Gaussian beam profile obtained at the maximum output power.

4. Conclusion

In conclusion, we present a detailed study on cryogenic spectroscopy and the first continuous-wave laser operation of 7.35 at.% Yb:YGG garnet crystal at cryogenic temperatures. An absorption cross-section of 1.7 10^{-20} cm^2 centered at 970.5 nm and emission cross-section of 6.5 × 10^{-20} cm^2 centered at 1024 nm at 120 K, respectively were determined. An efficient CW laser was achieved, we recorded a maximum output power of 17.50 W using 50% TOC. Under the given experimental conditions, an optimum laser operation temperature was found to be 120 K with output power 5 times better than for laser operating at 200 K. With respect to the absorbed power, a slope efficiency of 87% and an optical-to-optical efficiency of 73% were obtained at 120 K. Future work will be focused on the passive Q-switching laser operation of this Yb:YGG garnet

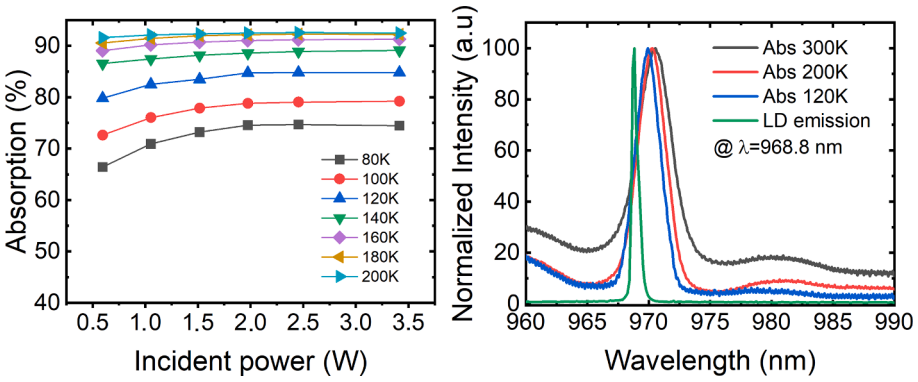

Fig. 6. (a) Yb:YGG pump absorption versus incident power for different crystal temperatures; (b) normalized absorption spectra of 7.35 at.% Yb:YGG crystal measured at 120, 200 and 300 K. The green curve shows the emission spectra of the 968.8 nm pump diode.

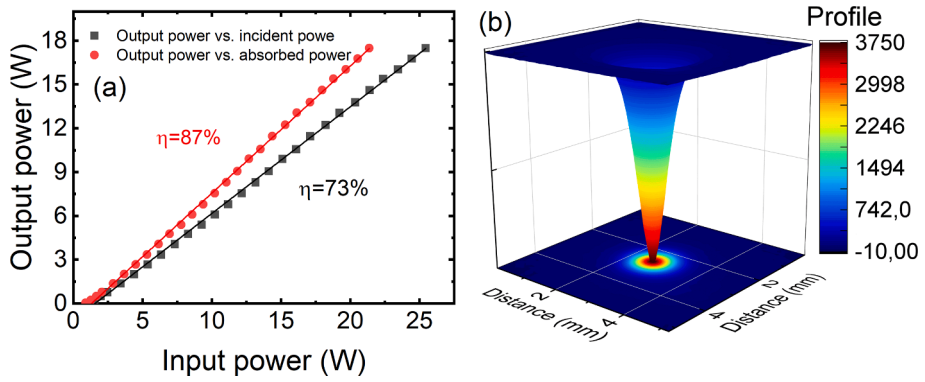

Fig. 7. (a) Output power versus incident and absorbed pump power at 120 K using 50% TOC; (b) Measured beam profile at maximum pump power using 50%TOC at 120 K.

at cryogenic temperatures using Cr^{3+}:YAG as saturable absorber.

CRediT authorship contribution statement

Sami Slimi: Conceptualization, Investigation, Writing – original draft. **Venkatesan Jambunathan:** Conceptualization, Investigation, Methodology, Writing – review & editing. **Ghassen Zin Elabedine:** . **Haohai Yu:** Investigation. **Huaijin Zhang:** Investigation. **Weidong Chen:** Investigation. **Rosa Maria Solé:** Investigation. **Magdalena Aguiló:** Funding acquisition. **Francesc Díaz:** Funding acquisition. **Martin Smrz:** Supervision, Resources. **Tomas Mocek:** Supervision, Funding acquisition. **Xavier Mateos:** Conceptualization, Supervision.

Declaration of Competing Interest

The authors declare that they have no known competing financial interests or personal relationships that could have appeared to influence the work reported in this paper.

Data availability

No data was used for the research described in the article.

Acknowledgments

This research article has been possible with the support of the Secretaria d'Universitats i Recerca del Departament d'Empresa i Coneixement de la Generalitat de Catalunya, the European Union (UE), and the European Social Fund (ESF) (2021 FI_B1 00170). Grant PID2019-108543RB-I00 funded by MCIN/AEI/10.13 039/501100011033. This work was co-financed by the European Regional Development Fund and the state budget of the Czech Republic (project HiLASE CoE: Grant No. CZ.02.1.01/0.0/0.0/15_006/0000674) and by the European Union's Horizon 2020 research and innovation programme under grant agreement No. 739573. And by Grant PECT "Cuidem el que ens uneix", operation 4 Sensòrica, Act 4 Fotònica" PR15-020174 co-financed by the European Regional Development Fund "ERDF A way of making Europe" through the ERDF Catalonia Operational Programme 2014-2020.

References

[1] S. Lei, X. Zhao, X. Yu, A. Hu, S. Vukelic, M.B.G. Jun, H.E. Joe, Y. Lawrence Yao, Y. C. Shin, Ultrafast Laser Applications in Manufacturing Processes: A State-of-the-Art Review, J. Manuf. Sci. Eng. Trans. ASME. 142 (2020), 031005.
[2] M.A. Ahmed, C. Roecker, A. Loescher, F. Bienert, D. Holder, R. Weber, V. Onuseit, T. Graf, High-power ultrafast thin-disk multipass amplifiers for efficient laser-based manufacturing, Adv. Opt. Technol. 10 (2021) 285–295.
[3] S. Chénais, F. Druon, S. Forget, F. Balembois, P. Georges, On thermal effects in solid-state lasers: The case of ytterbium-doped materials, Prog. Quantum Electron. 30 (2006) 89–153.
[4] Z.-L. Lin, W.-Z. Xue, H.-J. Zeng, G. Zhang, P. Zhang, Z. Chen, Z. Li, V. Petrov, P. Loiko, X. Mateos, H. Lin, L. Wang, W. Chen, W. Chen, Kerr-lens mode-locked ytterbium-activated orthoaluminate laser, Opt. Lett. 47 (2022) 3027–3030.
[5] W. Chen, W. Chen, Z.-L. Lin, W.-Z. Xue, H.-J. Zeng, G. Zhang, P. Loiko, Y. Zhao, X. Xu, J. Xu, X. Mateos, H. Lin, L. Wang, V. Petrov, Kerr-lens mode-locked Yb:$YAlO_3$ laser generating 24-fs pulses at 1085 nm, Opt. Lett. 47 (2022) 4728–4731.
[6] H. Zeng, H. Zeng, H. Zeng, H. Lin, H. Lin, Z. Lin, L. Zhang, Z. Lin, G. Zhang, V. Petrov, P. Loiko, X. Mateos, X. Mateos, L. Wang, L. Wang, W. Chen, W. Chen, W. Chen, Diode-pumped sub-50-fs Kerr-lens mode-locked Yb:GdYCOB laser, Opt. Express 29 (2021) 13496–13503.
[7] S. Chénais, F. Druon, F. Balembois, P. Georges, A. Brenier, G. Boulon, Diode-pumped Yb:GGG laser: comparison with Yb:YAG, Opt. Mater. (Amst) 22 (2003) 99–106.
[8] M.D. Serrano, J.O. Álvarez-Pérez, C. Zaldo, J. Sanz, I. Sobrados, J.A. Alonso, C. Cascales, M.T. Fernández-Díaz, A. Jezowski, Design of Yb^{3+} optical bandwidths by crystallographic modification of disordered calcium niobium gallium laser garnets, J. Mater. Chem. C. 5 (2017) 11481–11495.
[9] R.L. Aggarwal, D.J. Ripin, J.R. Ochoa, T.Y. Fan, Measurement of thermo-optic properties of $Y_3Al_5O_{12}$, $Lu_3Al_5O_{12}$, $YAlO_3$, $LiYF_4$, $LiLuF_4$, BaY_2F_8, $KGd(WO_4)_2$, and $KY(WO_4)_2$ laser crystals in the 80–300K temperature range, J. Appl. Phys. 98 (2005), 103514.
[10] S.P. David, V. Jambunathan, F. Yue, B.J. Le Garrec, B.J. Le Garrec, A. Lucianetti, T. Mocek, Laser performances of diode pumped Yb:Lu_2O_3 transparent ceramic at cryogenic temperatures, Opt. Mater. Express 9 (2019) 4669–4676.
[11] D.C. Brown, The promise of cryogenic solid-state lasers, IEEE J. Sel. Top. Quantum Electron. 11 (2005) 587–599.
[12] H. Yu, K. Wu, B. Yao, H. Zhang, Z. Wang, J. Wang, Y. Zhang, Z. Wei, Z. Zhang, X. Zhang, M. Jiang, Growth and characteristics of Yb-doped $Y_3Ga_5O_{12}$laser crystal, IEEE J. Quantum Electron. 46 (2010) 1689–1695.
[13] K. Wu, Z. Zhou, H. Zhang, R.I. Boughton, H. Yu, X. Tian, J. Liu, Y. Wang, J. Wang, L. Hao, $Lu_3Ga_5O_{12}$ crystal: exploration of new laser host material for the ytterbium ion, JOSA B 29 (2012) 2320–2328.
[14] C. Xu, Y. Zhang, Z. Wei, Z. Zhang, J. Wang, B. Zhou, J. Wang, Y. Zou, K. Wu, B. Yao, H. Zhang, D. Li, H. Yu, Diode-pumped passively mode-locked Yb:$Y_3Ga_5O_{12}$ laser, Opt. Lett. 34 (2009) 3316–3318.
[15] W. Han, Y. Ma, X. Dou, L. Wang, H. Xu, J. Liu, Passive Q-switching laser properties of Yb:$Re_3Ga_5O_{12}$ (Re = Y, Lu, Gd) garnets with GaAs semiconductor saturable absorber, Opt. Commun. 423 (2018) 1–5.
[16] Y. Zhang, Z. Wei, Z. Zhang, Q. Wang, L. Lv, H. Zhang, D. Li, H. Yu, J. Wang, Diode-pumped efficient continuous-wave Yb:$Y_3Ga_5O_{12}$ laser at 1035 nm, Opt. Lett. Vol. 36, Issue 4, Pp. 472-474. 36 (2011) 472–474.
[17] J.M. Serres, V. Jambunathan, P. Loiko, X. Mateos, H. Yu, H. Zhang, J. Liu, A. Lucianetti, T. Mocek, K. Yumashev, U. Griebner, V. Petrov, M. Aguiló, F. Díaz, Microchip laser operation of Yb-doped gallium garnets, Opt. Mater. Express 6 (2016) 46–57.
[18] J.M. Serres, P. Loiko, X. Mateos, H. Yu, H. Zhang, J. Liu, K. Yumashev, U. Griebner, V. Petrov, M. Aguiló, F. Díaz, Q-switching of Yb:YGG, Yb:LuGG and Yb:CNGG lasers by a graphene saturable absorber, Opt. Quantum Electron. 48 (2016) 1–7.
[19] R. Pappalakdo, D.L. Wood, Spectrum of Yb^{3+} in Yttrium Gallium Garnet, J. Chem. Phys. 33 (1960) 1734–1742.
[20] V. Jambunathan, A. Endo, L. Horackova, A. Lucianetti, T. Mocek, J. Sulc, T. Miura, H. Jelínková, Spectroscopic and lasing characteristics of Yb:YGAG ceramic at cryogenic temperatures, Opt. Mater. Express 5 (2015) 1289–1295.
[21] P. Veitch, M. Ganija, J. Munch, D. Ottaway, Cryogenic, high power, near diffraction limited, Yb:YAG slab laser, Opt. Express 21 (2013) 6973–6978.
[22] S. Paul David, V. Jambunathan, F. Yue, A. Lucianetti, T. Mocek, Diode pumped cryogenic Yb:$Lu_3Al_5O_{12}$ laser in continuous-wave and pulsed regime, Opt. Laser Technol. 135 (2021), 106720.
[23] D. Rand, J. Hybl, T.Y. Fan, Cryogenic lasers, Handb. Solid-State Lasers Mater. Syst. Appl. (2013) 525–550.

[24] V. Jambunathan, L. Horackova, P. Navratil, A. Lucianetti, T. Mocek, Cryogenic Yb: YAG laser pumped by VBG-Stabilized narrowband laser diode at 969 nm, IEEE Photonics Technol. Lett. 28 (2016) 1328–1331.

[25] S.A. Payne, L.L. Chase, L.K. Smith, W.L. Kway, W.F. Wyers, Infrared Cross-Section Measurements for Crystals Doped with Er^{3+}, Tm^{3+}, and Ho^{3+}, IEEE J. Quantum Electron. 28 (1992) 2619–2630.

[26] P. Deng, M. Bass, F. Gan, J. Dong, Y. Mao, Dependence of the Yb^{3+} emission cross section and lifetime on temperature and concentration in yttrium aluminum garnet, JOSA B 20 (2003) 1975–1979.